Semiconductor materials and radiation detection

Alan Owens

Science Payload and Advanced Concepts Office, SCI-AT, ESA/ESTEC, Postbus 299, 2200AG Noordwijk, The Netherlands. E-mail: aowens@rssd.esa.int

While Si and Ge have become detection standards for X-ray and γ-ray spectroscopy in the laboratory, their use for an increasing range of applications is becoming marginalized by one or more of their physical limitations; namely the need for ancillary cooling systems or bulky cryogenics, their modest stopping powers and radiation intolerance. Wide band-gap compounds offer the ability to operate in a range of chemical, thermal and radiation environments while still maintaining sub-keV spectral resolution at X-ray wavelengths. In addition, these materials encompass such a wide range of physical properties that it is technically feasible to engineer materials to specific applications. However, while compound materials are used routinely in the optical and infrared wave bands, their development at hard X- and γ-ray wavelengths has been plagued by material and fabrication problems. In this paper an overview of suitable materials is presented and the current progress in producing X- and γ-ray radiation detectors is reviewed.

Keywords: compound semiconductors; radiation detectors; X-rays; γ-rays.

1. Introduction

Semiconductor materials can generally be grouped into two categories. These are the elemental semiconductors, Si and Ge, which are derived from elements in group IV of the periodic table, and compound semiconductors, the most common of which are derived from groups III and V (*e.g.* GaAs, InP) and groups II and VI (*e.g.* CdTe) of the periodic table. Compound semiconductors are so useful because of the sheer range of compounds available. This is illustrated in Table 1, in which we list the semiconductors available as a function of group and band-gap energy. In addition to binary materials (such as GaAs or InP), most compounds are also soluble within each other, making it possible to synthesize ternary (*e.g.* AlGaAs, HgCdTe), quaternary (*e.g.* InGaAsP, InGaAlP) and higher-order solutions, simply by alloying binary compounds together. The basic problem in producing detector-grade material is the difficulty of growing chemically pure and structurally perfect crystals with exact stoichiometry.

For radiation detection, compound semiconductors have a number of distinct advantages over their elemental counterparts, arising from the wide range of stopping powers and band gaps available. For example, band-gap energies range from $\sim$1.35 to $\sim$2.6 eV and average atomic numbers from $\sim$30 to $\sim$90 (see Table 1). This suggests that it may be possible to mix and match available band gaps and stopping powers, which in turn implies that materials can be targeted for specific applications in radiation detection. For example, within a given target spectral resolution and detection efficiency, it is usually possible to select from a range of stopping powers. Choosing materials with the largest stopping powers enables thinner detectors to be produced with resulting benefits in radiation tolerance (which is a bulk effect) and lower leakage currents. Alternatively, choosing smaller stopping powers will increase scattering efficiency, which is a requirement for polarimetry measurements. These compounds can also be tailored towards tissue equivalence. By careful choice of both band gap and stopping power it is possible to fabricate detectors with a very wide dynamic range but sub-keV energy resolution in the soft X-ray band and tens of keV in the γ-ray band. For space research this is particularly attractive since it has mass and cost benefits in spacecraft design in that by using denser materials smaller detection systems can be fabricated without losing spectral acuity. Finally, unlike Si and Ge whose electronic and chemical properties are 'fixed', those of compound semiconductors can be modified by band-gap engineering. Specifically, the energy gap between the valence and conduction states is defined by the interatomic distance and the electronegativity of the component atoms. Changing the composition of an alloy changes its average lattice constant to reflect the different atomic bonding radii of the constituent elements. This changes the band-gap energy, which in turn alters the properties of the material. A specific example of how this is useful for radiation detector applications is $Cd_{(1-x)}Zn_xTe$ in which adding a few percent Zn to CdTe not only increases the band-gap energy but also increases the energy of defect formation and its mechanical strength. Consequently, leakage currents and resistivities are correspondingly higher.

doi:10.1107/S0909049505033339 **143**

detectors

Table 1
Compound semiconductor materials listed by group and in order of increasing band-gap energy ranging from the near-IR to XUV wavelengths.

Band-gap energy (eV)	Elemental group IVB	Binary IV–IV compounds	Binary III–V compounds	Binary II–VI compounds	Binary IV–VI compounds	Binary n–VIIB compounds	Ternary compounds
0.00–0.25	Sn		InSb†	HgTe			HgCdTe
0.25–0.50		SiGe	InAs	HgSe	PbSe, PbS, PbTe		
0.50–0.75	Ge‡		GaSb				InGaAs
0.75–1.00		SiGe					
1.00–1.25	Si‡				SnS		
1.25–1.50			GaAs‡, InP‡	CdTe‡			AlInAs
1.50–1.75			AlSb	CdSe‡			AlGaAs
1.75–2.00			BP, InN			BiI$_3$†	CdZnTe‡, CdZnSe‡, InAlP
2.00–2.25		SiC‡	AlAs	HgS		HgI$_2$‡	CdMnTe‡
2.25–2.50			GaP†, AlP	ZnTe, CdS		PbI$_2$‡	TlBrI‡, InAlP, TlPbI$_3$
2.50–2.75				ZnSe†		TlBr‡	HgBrI
2.75–3.00				MnSe			
3.00–3.25				MnTe			
3.25–3.50				MgTe, MnS			
3.50–3.75				MgSe, ZnS			
3.75–4.00							
4.00–4.25							
4.25–4.50				MgS			
4.50–4.75							
4.75–5.00							
5.00–5.25							
5.25–5.50	C†						
5.50–5.75							
5.75–6.00			BN				
6.00–6.25			AlN				
6.25–6.50							
6.50–6.75							
6.75–7.00							

† Compounds which have shown some response to radiation. ‡ Materials for which spectroscopic measurements (*i.e.* $E/\Delta E > 1$) have been made at X-ray wavelengths. Here, ΔE is the FWHM energy resolution at energy E.

2. Radiation detection using compound semiconductors

All semiconductor detectors operate as solid-state ionization chambers. In Fig. 1 we illustrate a simple planar detector geometry. Ionizing radiation absorbed in the sensitive volume excites electron–hole pairs in direct proportion to the energy deposited (*i.e.* $n_o = E_o/\varepsilon$, where n is the number of electron–hole pairs generated, E_o is the energy deposited and ε is the average energy consumed to create an electron–hole pair). Applying an electric field across the detector causes the liberated carriers to drift towards the anode and cathode with drift velocities v_e and v_h, creating an induced charge on the electrodes and by current continuity into the electronics. The induced charge Q_{ind} is given by the Shockley–Ramo theorem (Shockley, 1938; Ramo, 1939) which makes use of the concept of a weighting potential. The weighting potential is defined as the potential that would exist in the detector with the collecting electrode held at unit potential while holding all other electrodes at zero potential. The theorem states that, regardless of the presence of space charge, the change in the induced charge ΔQ_{ind} and the current i at an electrode caused by a charge q moving from x_i to x_f are given by

$$\Delta Q_{ind} = \int_{x_i}^{x_f} q E_w(x)\, dx = -q\big[V_w(x_f) - V_w(x_i)\big]$$
$$i = dQ/dt = q v\, E_w, \tag{1}$$

where $V_w(x)$ and $E_w(x)$ are the weighting potential and field at position x. The total induced charge will actually be the sum of the induced charges owing to the electron and holes. The integration of these charges along their respective pathlengths gives the total charge, Q. In the absence of trapping, $Q = Q_o = -qn_o$, the original charge created, which in turn is proportional to the energy of the incident photon. However, in any semiconductor some density of electron and hole traps are always present and these result in a loss of carriers and therefore charge at the electrodes. For compound semiconductors, crystal growth practices lead to a much higher density of traps than in the elemental semiconductors and hence shorter lifetimes. For example, in CdZnTe, typical lifetimes are $\tau_e = 3 \times 10^{-6}$ s and $\tau_h = 5 \times 10^{-8}$ s. Because the hole lifetime is much shorter than the hole transit time, the induced charge is significantly reduced and is now dependent upon the depth of interaction, x_o. In the case of a uniform electric field and negligible de-trapping, the fraction of charge that is induced at the electrodes is best described by the charge collection efficiency (CCE), which is given by the Hecht equation (Hecht, 1932),

$$CCE = Q/Q_o = (\lambda_e/L)\big\{1 - \exp\big[-(L - x_o)/\lambda_e\big]\big\} + (\lambda_h/L)\big[1 - \exp(-x_o/\lambda_h)\big], \tag{2}$$

where L is the detector thickness, x_o is the distance from the cathode to the point of charge creation, and λ_e and λ_h are the carrier drift lengths in the applied electric field, $\mathcal{E}$, given by $\lambda_e = \mu_e \tau_e \mathcal{E}$ and $\lambda_h = \mu_h \tau_h \mathcal{E}$. Here, μ_e and μ_h are the electron and hole mobilities and τ_e and τ_h are the corresponding lifetimes.

It follows from (2) that the CCE depends not only on λ_e and λ_h but also on the location where the charge was created. Since the interaction points of incident photons is essentially random at intermediate and high energies, being weighted by the classical exponential absorption law, the width of the peak in the energy spectrum broadens to a degree governed by the ratios λ_e/L and λ_h/L.

In characterizing materials, perhaps the most useful figure of merit is the mobility–lifetime product ($\mu\tau$), which is directly related to the drift length. Poorer mt products result in shorter drift lengths and therefore smaller λ/L, which in turn limit the maximum size and energy range of detectors. For the elemental semiconductors, $\mu\tau$ is of the order of unity cm^2 V^{-1} for both electrons and holes, whereas for compound semiconductors it rarely reaches greater than a few times 10^{-4} cm^2 V^{-1} for electrons and 10^{-5} cm^2 V^{-1} for holes, and these figures become worse with increasing Z (see Table 2). The cause can usually be traced to trapping centers caused by impurities, vacancies and structural irregularities (*e.g.* dislocations), or, for the softer materials, plastic deformation caused by mechanical damage during fabrication.
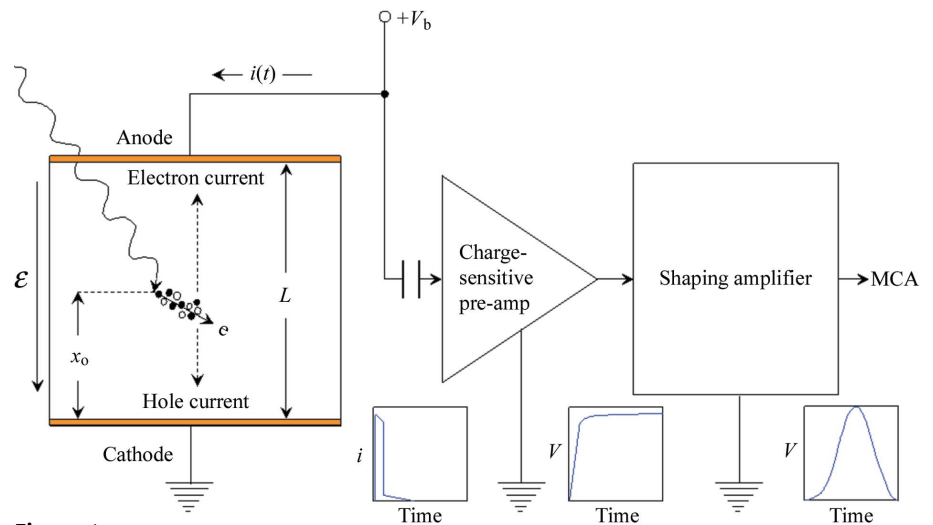

Figure 1
Left: schematic of a simple planar detection system. For completeness we also show the signal chain and the evolution of currents and voltages. Ionizing radiation absorbed in the sensitive volume generates electron–hole pairs in direct proportion to the energy deposited. These are subsequently swept towards the appropriate electrode by the electric field induced by the bias voltage V_b.

3. Spectral broadening in radiation detection systems

In addition to broadening caused by poor charge collection, the width of the full energy peak, ΔE, is also broadened by the statistics of carrier generation (Fano noise) and by electronic noise. For most compound semiconductors, however, these components are generally far less important than the noise owing to incomplete charge collection, except for thin detectors where $\lambda_e/L \gg 1$. The energy resolution, ΔE, of the system is defined as the full width at half-maximum of the energy-loss distribution resulting from exposure to mono-energetic radiation. The width of the energy-loss spectrum, in turn, results from the convolution of the probability distributions of the various noise components. For an infinitely thin detector, three terms tend to dominate,

$$\Delta E = f(\sigma_F^2, \sigma_e^2, \sigma_c^2) \quad (keV), \tag{3}$$

where σ_F^2 is the variance of the noise owing to carrier generation or Fano noise, σ_e^2 is the variance of the noise owing to the leakage current and amplifier noise, and σ_c^2 is the variance of the noise owing to incomplete charge collection owing to carrier trapping. The contribution owing to Fano noise, ΔE_F, is calculated from

$$\Delta E_F = 2.355\left(\sigma_F^2\right)^{1/2} = 2.355(FE\varepsilon)^{1/2} \quad (keV), \tag{4}$$

where F is the Fano factor, ε is the energy to create an electron–hole pair and E is the incident energy. The electronic noise component, ΔE_e, is given by

$$\Delta E_e = 2.355\left(I\tau\varepsilon^2 A/e + \sigma_a^2\right)^{1/2} \quad (keV), \tag{5}$$

where I is the leakage current, e is the electronic charge, A is a constant depending on the type of signal shaping, τ is the shaping time and σ_a^2 is the variance of the amplifier shot noise which depends on the actual design and specifically the capacitive loading of the front-end electronics. For the Gaussian shaping typically used in spectroscopy, $A = 0.875$.

The functional form of ΔE_c is much more difficult to predict, since it is intimately dependent on the trap density distribution as well as the charge diffusion and collection properties of the detector. For the case of $\lambda_e \neq \lambda_h$, which is invariably true for compound semiconductors, Iwanczyk *et al.* (1992) have arrived at the following analytic form for the relative broadening,

$$\left(\frac{\sigma_c}{E}\right)^2 = \frac{2\lambda_e^2\lambda_h^2}{L^3(\lambda_e - \lambda_h)}\left[\exp(-L/\lambda_e) - \exp(-L/\lambda_h)\right]$$
$$- \frac{1}{L^4}\left\{\lambda_e^2\left[\exp(-L/\lambda_e) - 1\right] + \lambda_h^2\left[\exp(-L/\lambda_h) - 1\right]\right\}^2$$
$$- \frac{\lambda_e^3}{2L^3}\left[\exp(-2L/\lambda_e) - 1\right] - \frac{\lambda_h^3}{2L^3}\left[\exp(-2L/\lambda_h) - 1\right], \tag{6}$$

assuming a uniform electric field. However, while (6) can be used to calculate the width ΔE_c, the shape of the pulse-height distribution can only be realistically evaluated by following the approach of Trammell & Walter (1969) in which the individual pulse heights in infinitesimal slices through the detector are summed over the detector thickness. For low trapping, the summed pulse-height distribution will be almost symmetric at low and intermediate energies and we can therefore assume ΔE_c is normally distributed. For this case,

Table 2
Room-temperature properties of wide-band-gap compound semiconductor materials suitable for hard X- and γ-ray detectors. The abbreviations are: C = Czochralski, CVD = chemical vapor deposition, LEC = liquid encapsulated Czochralski, THM = traveler heater method, BM = Bridgman method, HPB = high-pressure Bridgman and VA = vertical ampoule method.

Material	Growth method	Atomic number	Density (g cm^{-3})	Band gap (eV)	E_{pair} (eV)	Resistivity (Ω cm)	$\mu\tau$ (e) product (cm^2 V^{-1})	$\mu\tau$ (h) product (cm^2 V^{-1})
Si	C	14	2.33	1.12	3.6	10^4	4×10^{-1}	2×10^{-1}
Ge	C	32	5.33	1.57	4.6	50	1	1
4H-SiC	CVD	14, 6	3.17	3.26	7.8	$>10^3$	$<5 \times 10^{-4}$	$<8 \times 10^{-5}$
GaAs	CVD	31, 33	5.32	1.43	4.2	10^{11}	10^{-2}	5×10^{-4}
InP	LEC	15, 49	4.78	1.43	4.2	10^6	5×10^{-6}	$<2 \times 10^{-5}$
CdTe	THM	48, 52	6.2	1.44	4.4	10^9	3×10^{-3}	2.6×10^{-4}
Cd$_{0.9}$Zn$_{0.1}$Te	HPB	48, 30, 52	5.78	1.57	4.6	10^{11}	7×10^{-3}	9×10^{-5}
PbI$_2$	BM	82, 53	6.2	2.3–2.6	4.9	10^{12}	8×10^{-6}	9×10^{-7}
HgI$_2$	VAM	80, 53	6.4	2.13	4.2	10^{13}	10^{-4}	4×10^{-5}
TlBr	BM	81, 35	7.56	2.68	6.5	10^{12}	3×10^{-5}	1.5×10^{-6}

several semi-empirical formulae have been proposed for the summed response. For example, Henck *et al.* (1970) derived an expression for planar detectors in which $\Delta E_c \propto E^{-1/2}$ whereas Owens (1985) predicted that $\Delta E_c \propto E$ for coaxial detectors. Because of the uncertainties in the functional form of ΔE_c and our imprecise knowledge of F, a semi-empirical approach is generally used to describe the resolution function in which

$$\Delta E = 2.355\left[F\varepsilon E + (\Delta E_e/2.355)^2 + a_1 E^{a_2}\right]^{1/2} \quad \text{(keV)}, \quad (7)$$

where the electronic noise component ΔE_e is generally measured directly using a precision pulser, and F, a_1 and a_2 are treated as semi-empirical constants determined by best-fitting. Equation (7) is found to fit the resolution functions of compound semiconductors reasonably well with the charge-trapping exponent, a_2, varying between 2 and 3. Recently, the validity of the functional form of the trapping term has been rigorously tested by Kozorezov *et al.* (2005), who derived a general analytical expression, which includes the effects of geometry. Interestingly, it can be expressed in the form $G(E)E^2$, in which the function $G(E)$ reduces to a constant when the 1/e absorption lengths become comparable with the detector thickness, which is invariably true for spectroscopic detectors.

4. Present detection systems

Of the 50 or so compounds available, less than half have been investigated as possible detection media. This is illustrated in Table 1, in which compounds that have shown a spectroscopic response to X-rays (*i.e.* $E/\Delta E > 1$) and those that have shown some response to radiation (usually MeV α-particles) are indicated. From the former group of compounds, only CdTe, CdZnTe and HgI$_2$ have matured sufficiently to produce commercially viable detection systems and another four are tantalizingly close. We describe these materials below. Their physical and electrical properties are listed in Table 2.

Cadmium zinc telluride [Cd$_{(1-x)}$Zn$_x$Te] is probably the most widely used compound semiconductor. It has a cubic zinc-blende-type lattice with atomic numbers close to that of CdTe and a density about three times that of Si. CdTe was originally

the focus of experimental study in the 1960s, until it was discovered that the addition of a few percent of zinc to the melt resulted in an increased band gap as well as the energy of defect formation. This in turn increases bulk resistivities and reduces the dislocation density, resulting in lower leakage currents and higher temperature operation. Specifically, resistivities of CdZnTe are between one and two orders of magnitude greater than that for CdTe and thus leakage currents are correspondingly lower. Additionally, CdZnTe tends not to suffer from the polarization effects normally associated with CdTe. The best spectral performances are achieved with a zinc fraction of $\sim$10%. Typical FWHM energy resolutions at 59.54 keV are in the 1–2 keV range at room temperature and decrease with decreasing temperature to a minimum resolution at $\sim$243 K (Owens *et al.*, 2002).

Mercuric iodide (HgI$_2$) has been investigated as a room-temperature X- and γ-ray detector since the early 1970s. Its wide band gap in conjunction with the high atomic number of its constituent atoms makes it an attractive material for room-temperature operable X- and particularly γ-ray spectrometers. In fact, since photoelectric absorption varies as Z^5, the specific sensitivity of HgI$_2$ is about ten times greater than that of Ge for energies >100 keV. HgI$_2$ belongs to the family of layered-structured heavy metal iodides. It is a relatively soft material that forms a tetragonal lattice at temperatures below 403 K. This is known as the α phase and the crystals appear red in color with a band-gap energy of 2.13 eV. At temperatures above 403 K, HgI$_2$ undergoes a phase transformation to an orthorhombic lattice (β phase) appearing yellow in color with a band-gap energy of 2.5 eV. However, when cooled below 403 K, the material undergoes a destructive phase transition to α-HgI$_2$. This precludes melt growth. The fabrication of a pn junction is usually not necessary, as dark currents are generally very low. While reported energy resolutions are typically in the keV region, a series of small planar detectors (5 mm^2, cylinder, 200 µm-thick) developed by Iwanczyk *et al.* (1989) have achieved energy resolutions of $\sim$200 eV FWHM at 5.9 keV at 273 K.

Gallium arsenide (GaAs) has a simple cubic lattice structure with a band gap sufficiently wide (1.42 eV) to permit room-temperature operation but small enough so that its

Fano-limited spectroscopic resolution is close to that of Si. Compared with other compounds, the performances of GaAs detection systems have steadily advanced, primarily owing to improvements in both bulk material properties and detector fabrication techniques. Schottky barrier detectors fabricated using semi-insulating GaAs have consistently demonstrated reasonable room-temperature performances. Recently, Owens, Peacock & Bavdaz (2003) fabricated a series of detectors from ultra-high-purity GaAs grown by chemical vapor phase deposition (CVPD). From the I/V characteristics the typical current densities at -100 V were <0.04 nA mm^{-2} at room temperature. This is about a factor of 3–100 lower than normally obtained with CVPD detectors and a factor of 10^3–10^4 lower than bulk detectors. The measured FWHM energy resolutions of a 0.8 mm^2 40 μm-thick device operated at 253 K were 435 eV FWHM at 5.9 keV and 670 eV FWHM at 59.54 keV. At room temperature the corresponding resolutions were 572 eV and 780 eV, respectively. Spectral resolutions of only 200 eV FWHM at 5.9 keV have been recorded for pixel detectors (250 μm × 250 μm × 40 μm), fabricated from the same base material (Owens, Bavdaz, Peacock *et al.*, 2001).

Silicon carbide (SiC) is currently being explored as a high-temperature Si alternative that is also chemical and radiation tolerant. It has several distinct advantages over Si in that it has twice the thermal conductivity and eight times the maximum breakdown field. The former property is important for producing thermally stable or high-power semiconductor devices, while the latter means that much higher biases can be applied, resulting in higher drift velocities and better charge collection. Structurally, SiC is a polymorph with over 200 polytypes possible. However, only three have properties suitable for X-ray detection, namely 3H, 4H and 6H,[1] and of these 4H has the best electrical properties. At present, the X-ray performance of prototype detectors is still relatively poor, with FWHM resolutions of 2.7 keV at 59.54 keV being reported (Bertuccio *et al.*, 2001). However, recent measurements with small pixel detectors have achieved room-temperature energy resolutions of 693 eV FWHM at 59.54 keV (Bertuccio *et al.*, 2003).

Indium phosphide (InP) is direct band-gap material whose structural and electronic properties are similar to Si and GaAs. It has a zinc-blende-type crystal structure, with a single non-destructive phase transition below the melting point making it amenable to standard growth techniques. It has one of the highest electron mobilities of any semiconductor material (about three times that of silicon) making it particularly suitable for applications where high-count-rate operation is desirable (*e.g.* at synchrotrons). Its band gap of 1.35 eV implies that detectors should operate at room temperature with a Fano-limited spectroscopic resolution close to that of Si, and its relatively large density (approximately twice that of Si) ensures high X-ray detection efficiency above 10 keV. Currently, for small detectors of area 3.1 mm^2 and thickness 180 μm, FWHM spectral resolutions of ~2.5 keV and 9.2 keV have been achieved at 5.9 keV and 59.54 keV, respectively, at a detector temperature of 213 K. At LN$_2$ temperature (103 K), these figures improve considerably to 911 eV at 5.9 keV and 2.5 keV at 59.54 keV (Owens, Peacock & Bavdaz, 2003).

For γ-ray applications there has been some effort to develop the heavier compounds with limited success, particularly lead, bismuth and thallium compounds from period VI of the periodic table. For example, PbI$_2$ has been investigated as a stable alternative to HgI$_2$ since it does not exhibit a destructive phase change between the melting point and room temperature and its density is similar. Unfortunately, while thin detectors yield good room-temperature X-ray performance (415 eV FWHM at 5.9 keV and 1.4 keV FWHM at 59.54 keV for a 1 mm^2 device; Shah *et al.*, 1996), their transport properties are so poor that detectors thicknesses are limited to ~200 μm. Therefore, there has been little incentive to develop PbI$_2$ for γ-ray applications over say HgI$_2$, or even lower Z compounds such as CdZnTe or GaAs. Better results have been obtained with TlBr, with FWHM room-temperature energy resolutions of 1.8 keV at 5.9 keV and 3.3 keV at 59.5 keV recorded for detectors of dimensions 2.8 mm × 2.8 mm × 0.8 mm (Owens, Bavdaz *et al.*, 2003). These resolutions were found to improve with decreasing temperature exhibiting a minimum near 243 K. At this temperature the FWHM energy resolutions were 800 eV at 5.9 keV and 2.3 keV at 59.54 keV. Although these detectors did not suffer from the stability problems normally associated with TlBr detectors (Owens, Bavdaz, Lisjutun *et al.*, 2001), they did display polarization effects (*i.e.* time-dependent changes in gain and spectral broadening), which were correlated with large energy depositions per unit time.

Finally, in Table 3 we summarize some of the best reported spectral resolutions at soft and hard X-ray wavelengths for each of the above materials.

5. Spectral enhancement techniques

For conventional radiation detectors fabricated from compound semiconductors, the wide disparity between the transport properties of the electron and holes means that detector performances are limited by the carrier with the poorest mobility–lifetime product ($\mu\tau$). Finite drift lengths introduce an energy-dependent depth term into the charge-collection process, which effectively limits maximum detector thicknesses to a few mm for spectroscopy applications. Since mobility is a fundamental material property, the only practical way of improving $\mu\tau$ products is to increase carrier lifetimes, which in turn depends greatly on detector material quality and stoichiometry. In analogy with gas counters, until the particular traps/defect(s) can be identified and corrected, a significant improvement in spectral acuity can be achieved using single-carrier collection techniques; in other words, discarding the carrier with the poorest transport properties, albeit at the expense of detection efficiency. Single-carrier sensing can be achieved electronically by pulse rise-time discrimination (Jordanov *et al.*, 1996), and single-carrier collection by careful

---

[1] The 'H' numbers describe the stacking sequence of tetrahedrally bonded SiC bi-layers.

detectors

Table 3
The best energy resolutions achieved with prototype planar detectors. Note that the figures are quoted for the collection of both carriers. Spectral enhancement techniques involving single-carrier collection have not been employed. The measurements were carried out under uniform illumination using ^{55}Fe and ^{241}Am radioactive sources. For completeness, we also list the resolutions at room temperature (RT) where possible, since there are many applications in which resolving power is not a primary requirement.

| Material	Detector size area, thickness	ΔE at 5.9 keV (eV)	ΔE at 59.5 keV (eV)	Reference
Si	0.8 mm^2, 500 µm	245 at 258 K	524	Owens, Peacock & Bavdaz (2003)
		750 at 288 K	800	
GaAs	0.8 mm^2, 40 µm	450 at 251 K	670	Owens, Peacock & Bavdaz (2003)
		572 at RT	780	
GaAs pixel	250 µm × 250 µm × 40 µm	219 at 243 K	468	Owens, Bavdaz, Peacock et al. (2001)
		266 at RT	487	
SiC-4H	2 mm^2, 30 µm		2700 at RT	Bertuccio et al. (2001)
SiC-4H pixel	0.3 mm^2, 50 µm		693 at RT	Bertuccio et al. (2003)
InP	3.142 mm^2, 200 µm	911 at 103 K	3050	Owens, Peacock & Bavdaz (2003)
		2480 at 213 K	9200	
CdTe	16 mm^2, 1.2 mm	310 at 213 K	600	Loupilov et al. (2001)
CdZnTe	3.142 mm^2, 2.5 mm	311 at 236 K	824	Owens et al. (2002)
		1508 at RT	2900	
HgI$_2$	5 mm^2, 200 µm	198 at 273 K	650	Iwanczyk et al. (1989)
PbI$_2$	1 mm^2, 50 µm	415 at RT	1380	Shah et al. (1996)
TlBr	3.142 mm^2, 800 µm	800 at 243 K	2300	Owens, Bavdaz et al. (2003)
		1800 at RT	3300	

design (*e.g.* hemispherical; Richter & Siffert, 1992) or coplanar grid detectors (Luke, 1995) or, in the case of pixel detectors, by exploiting the small-pixel effect (Barrett *et al.*, 1995). In fact, such techniques have been widely applied to CdZnTe detectors to overcome poor hole transport. From Table 2 we note that the $\mu\tau$ product for electrons is usually about one to two orders of magnitude greater than that for the holes, which means that for present detection systems the electrons are almost fully collected for interactions occurring throughout the detector volume and that spectral tailing is almost exclusively due to holes. We discuss two of these techniques below.

5.1. Rise-time discrimination

Rise-time discrimination (RTD) is a relatively simple method (Jordanov *et al.*, 1996) of improving spectral shape and relies on the fact that for widely different transport properties the rise times of the current pulses owing to the electrons and holes are quite different. With reference to Fig. 1, the time taken for an electron and a hole to traverse the detector width L is

$$t_e = L/\mu_e E \quad \text{and} \quad t_h = L/\mu_h E, \tag{8}$$

from which we can see that the electron and hole transit times are directly dependent on carrier mobilities. Consider interactions in the detector volume. Then, since $\mu_e \gg \mu_h$, the rising edge of the detector signal will be composed of a fast component owing to the electrons and a slow component owing to the holes. In RTD methods, all pulses with a rise time exceeding a pre-set threshold are rejected; in fact, all those events that would normally lie in the tail. The effect of RTD is demonstrated in Fig. 2, in which we show the measured response of a 3 mm × 3 mm × 2 mm CdZnTe detector (Owens, Buslaps, Erd *et al.*, 2005). While the resolution is improved (from 1 keV FWHM at 59.54 keV to 700 eV), by using RTD the efficiency is lower than that expected from the
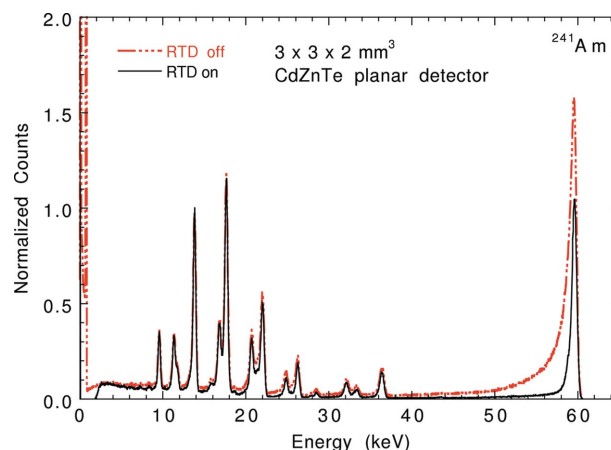
Figure 2
Two ^{241}Am spectra taken with an Amptek 3 mm × 3 mm × 2 mm CdZnTe detector, illustrating the effectiveness of RTD (Owens, Buslaps, Erd *et al.*, 2005). From the figure we see that the hole tailing is substantially reduced in the case where RTD is used and in fact the FWHM energy resolution improves from 1 keV to 700 eV at 59.54 keV. However, an energy-dependent decrease in efficiency is also apparent.

physical dimensions of the detector, since many counts are rejected. This is also demonstrated in Fig. 2 in which we can see that the amplitude of the lowest peak at ~9 keV is essentially the same in both spectra, since the entire signal is due to the electrons. However, there is an increasing loss of counts in subsequent peaks of the RTD-on spectrum as the energy increases. In fact, the ratio of counts in the 60 keV photopeak (*i.e.* RTD-on/RTD-off) is ~0.35 and the ratio of peak heights is ~0.65.

Since both rise time and signal amplitude are correlated with the depth of interaction, one can use these measurements to deduce charge collection efficiency and thus improve spectroscopic performance. Such methods are termed biparametric methods. In practice, it is achieved by plotting rise time as a function of pulse amplitude and energy, from which

one can generate a set of correction factors. The measured induced charge is then multiplied by the appropriate correction factor, yielding a corrected pulse amplitude. This technique permits high resolution with little loss of sensitive volume. For example, Verger *et al.* (2001) report measuring a FWHM energy resolution of 6.5% at 122 keV using a room-temperature 4 mm × 4 mm × 6 mm CdZnTe detector with standard planar electrodes. The quoted acceptance efficiency was >80%. However, there are disadvantages. Firstly, the electronics are complicated, and, secondly, since the pulse-height deficit varies non-linearly with rise time, the technique is only valid over a limited detector depth. Systems have been developed that apply non-linear corrections and effectively use the entire depth of the detector. However, their complexity and the difficulty of calibration make them uncommercial at this time.

5.2. Co-planar grid detectors

The co-planar grid technique (Luke, 1995) is essentially an evolution of the classical Frisch grid, introduced to reduce position-dependent charge-collection effects in gas detectors. By including a grid within the gas volume near the anode of the device, it is possible to bias the electrodes such that electrons are drifted towards the anode through the grid and positive ions are drifted in the opposite direction. According to the Shockley–Ramo theorem, the induced charge on the anode is primarily from electrons moving from the grid to the anode, hence the photon interaction position dependence of the pulse shape is greatly reduced. A similar concept has been shown to work with semiconductor devices, *i.e.* coplanar grid devices. The anode electrodes take the form of inter-digitated grids that are connected to separate charge-sensitive pre-amplifiers. An electric field is established in the detector bulk by applying bias to the cathode, which is a full-area contact located on the side opposite the grid electrodes. The two grid preamplifiers are connected to a subtraction circuit to produce a difference signal. Bias is applied between the grid electrodes so that one of the grids preferentially collects charge. Charge motion within the bulk of the detector is sensed equally by the
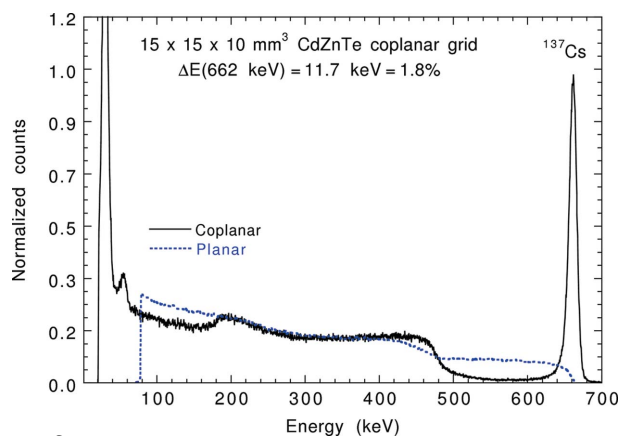
grid electrodes and the difference is essentially zero. However, when charge approaches the anode, the grid signals begin to differ and a signal is registered at the output of the difference circuit. In a well designed detector and in the absence of electron trapping, the magnitude of the difference signal is the same no matter where the charge is generated in the device. This results in a large improvement in performance for γ-ray spectroscopy when compared with conventional planar device technology. In fact, operating the grids as a simple planar detector results in no spectroscopic signal, but when operated in the co-planar geometry the results are quite dramatic and are illustrated in Fig. 3 (from Owens, Buslaps, Gostilo *et al.*, 2005).

6. Discussion and conclusions

While novel designs can improve energy resolution, ultimately carrier transport still limits the maximum detection volume. For the transport properties appropriate for CdZnTe, this is about 10 cm^3. Thus, ultimately the quality of the material has to be improved if a substantial increase in detector volume is to be achieved, sufficient to produce an effective γ-ray detector. In the longer term, material improvements must be paralleled by corresponding developments in heterostructure and quantum heterostructure technology, provided of course strain is not a limiting factor. Heterostructures may solve the problem of contacting by building up a series of semiconductor layers until it is possible to satisfy the relationship that the work function of the metal contact is less than that of the semiconductor (*i.e.* $\varphi_m < \varphi_s$) for n-type material and greater than that of the semiconductor for p-type material. At the present time, the first purpose-built heterostructures for X-ray applications are being reported in the literature (Silenas *et al.*, 2003).

Figure 3
Comparison of pulse-height spectra measured with a 2.25 cm^3 device (15 mm × 15 mm × 10 mm) when operated as a planar detector and as a coplanar grid detector (Owens, Buslaps, Gostilo *et al.*, 2005).

References

Barrett, H., Eskin, J. & Barber, H. (1995). *Phys. Rev. Lett.* **75**, 156–159.

Bertuccio, G., Casiraghi, R., Gatti, E., Maiocchi, D., Nava, F., Canali, C., Cetronio, A. & Lanzieri, C. (2003). *Mater. Sci. Forum*, **433–436**, 941–944.

Bertuccio, G., Casiraghi, R. & Nava, F. (2001). *IEEE Trans. Nucl. Sci.* NS-**481**, 232–233.

Hecht, K. (1932). *Z. Phys.* **77**, 235–245.

Henck, R., Gutknecht, D., Siffert, P., De Laet, L. & Shoenmaekers, W. (1970). *IEEE Trans. Nucl. Sci.* NS-**17**, 149–159.

Iwanczyk, J. S., Schnepple, W. F. & Masterson, M. J. (1992). *Nucl. Instrum. Methods*, A**322**, 421–426.

Iwanczyk, S., Yang, Y. J., Bradley, J. G., Conley, J. M., Albee, A. L. & Economou, T. E. (1989). *IEEE Trans. Nucl. Sci.* NS-**36**, 841–845.

Jordanov, V. T., Pantazis, J. A. & Huber, A. C. (1996). *Nucl. Instrum. Methods*, A**380**, 353–357.

Kozorezov, A., Wigmore, K., Owens, A., den Hartog, R., Peacock, A. & Al-Jawhari, H. A. (2005). *Nucl. Instrum. Methods*, A**546**, 209–212.

Loupilov, L., Sokolov, A. & Gostilo, V. (2001). *Rad. Phys. Chem.* **61**, 463–464.

Luke, P. N. (1995). *IEEE Trans. Nucl. Sci.* NS-**42**, 207–213.

Owens, A. (1985). *Nucl. Instrum. Methods*, A**238**, 473–478.

detectors

Owens, A., Bavdaz, M., Andersson, H., Gagliardi, T., Krumrey, M., Nenonen, S., Peacock, A. & Taylor, I. (2002). *Nucl. Instrum. Methods*, A**484**, 242–250.

Owens, A., Bavdaz, M., Brammertz, G., Gostilo, V., Graafsma, H., Krumrey, M., Lisjutin, I., Peacock, A., Puig, A., Sipila, H. & Zatoloka, S. (2003). *Nucl. Instrum. Methods*, A**497**, 370–380.

Owens, A., Bavdaz, M., Lisjutun, I., Peacock, A. & Zatoloka, S. (2001). *Nucl. Instrum. Methods*, A**458**, 413–417.

Owens, A., Bavdaz, M., Peacock, A., Poelaert, A., Andersson, H., Nenonen, S., Tröger, L. & Bertuccio, G. (2001). *J. App. Phys.* **90**, 5376–5381.

Owens, A., Buslaps, T., Erd, C., Graafsma, H., Hijmering, R., Lumb, D. & Welter, E. (2005). *Nucl. Instrum. Methods.* Submitted.

Owens, A., Buslaps, T., Gostilo, V., Graafsma, H., Hijmering, R., Kozorezov, A., Loupilov, A., Lumb, D. & Welter, E. (2005). *Nucl. Instrum. Methods.* Submitted.

Owens, A., Peacock, A. & Bavdaz, M. (2003). *Proc. SPIE*, **4851**, 1059–1070.

Ramo, S. (1939). *Proc. IRE*, **27**, 584–585.

Richter, M. & Siffert, P. (1992). *Nucl. Instrum. Methods*, A**322**, 529–537.

Shah, K., Olschner, F., Moy, L., Bennett, P., Misra, M., Zhang, J., Squillante, M. & Lund, J. (1996). *Nucl. Instrum. Methods*, A**380**, 266–270.

Shockley, W. (1938). *J. Appl. Phys.* **9**, 635–636.

Silenas, S., Pozela, K., Dapkus, L., Jasutis, V., Juciene, V., Pozela, J. & Smith, K. (2003). *Nucl. Instrum. Methods*, A**509**, 30–33.

Trammell, R. & Walter, F. J. (1969). *Nucl. Instrum. Methods*, **76**, 317–321.

Verger, L., Boitel, M., Gentet, M. C., Hamelin, R., Mestais, C., Mongellaz, F., Rustique, J. & Sanchez, G. (2001). *Nucl. Instrum. Methods*, A**458**, 297–309.